

Characteristics and triggering mechanisms of early negative Indian Ocean Dipole

Yue Fang^{1, 2, 3*}, Shuangwen Sun^{1, 2, 3}, Yongcan Zu^{1, 2, 3}, Jianhu Wang^{1, 3}, Lin Feng^{1, 2, 3}

¹ First Institute of Oceanography, and Key Laboratory of Marine Science and Numerical Modeling, Ministry of Natural Resources, Qingdao 266061, China

² Laboratory for Regional Oceanography and Numerical Modeling, Qingdao Marine Science and Technology Center, Qingdao 266237, China

³ Shandong Key Laboratory of Marine Science and Numerical Modeling, Qingdao 266061, China

Received 21 September 2023; accepted 14 December 2023

© Chinese Society for Oceanography and Springer-Verlag GmbH Germany, part of Springer Nature 2024

Abstract

Negative Indian Ocean Dipole (nIOD) can exert great impacts on global climate and can also strongly influence the climate in China. Early nIOD is a major type of nIOD, which can induce more pronounced climate anomalies in summer than La Niña-related nIOD. However, the characteristics and triggering mechanisms of early nIOD are unclear. Our results based on reanalysis datasets indicate that the early nIOD and La Niña-related nIOD are the two major types of nIOD, and the former accounts for over one third of all the nIOD events in the past six decades. These two types of nIODs are similar in their intensities, but are different in their spatial patterns and seasonal cycles. The early nIOD, which develops in spring and peaks in summer, is one season earlier than the La Niña-related nIOD. The spatial pattern of the wind anomaly associated with early nIOD exhibits a winter monsoon-like pattern, with strong westerly anomalies in the equatorial Indian Ocean and easterly anomalies in the northern Indian Ocean. Opposite to the triggering mechanism of early positive IOD, the early nIOD is induced by delayed Indian summer monsoon onset. The results of this study are helpful for improving the prediction skill of IOD and its climate impacts.

Key words: Indian Ocean Dipole (IOD), triggering mechanism, Indian summer monsoon, seasonal cycle, negative IOD

Citation: Fang Yue, Sun Shuangwen, Zu Yongcan, Wang Jianhu, Feng Lin. 2024. Characteristics and triggering mechanisms of early negative Indian Ocean Dipole. *Acta Oceanologica Sinica*, 43(3): 59–65, doi: 10.1007/s13131-023-2294-y

1 Introduction

Indian Ocean Dipole (IOD) is an air-sea coupled phenomenon occurring in the tropical Indian Ocean (Saji et al., 1999; Webster et al., 1999). It is the dominant mode of interannual climate variability in the Indian Ocean, and exerts great impacts on local climate and may influence various parts of the globe via atmospheric bridge effects (Saji and Yamagata, 2003).

There are two types of IOD according to its phases: the positive IOD (pIOD) and the negative IOD (nIOD). A positive IOD, which is tightly coupled with the equatorial easterly wind anomaly, is characterized by anomalous cooling in sea surface temperature (SST) in the southeastern tropical Indian Ocean and anomalous warming in SST in the western tropical Indian Ocean. While during nIOD, the spatial pattern of SST anomalies (SSTA) is opposite. The characteristics and mechanisms of pIOD have been extensively studied previously, but the understandings about nIOD are still limited compared with those about pIOD.

A large number of observations show that the nIOD can exert strong impacts on climate and marine environment. The nIOD can induce heavy rainfall and flooding in Indonesia and Australia (Risbey et al., 2009; Hatmaja et al., 2019), and significantly reduce the rainfall in eastern Africa (WMO, 2017; Lim and Hen-

don, 2017). Strong nIOD events in 2016 and 2021 both caused extreme droughts in eastern Africa, leading to a range of problems such as water security, food crises, and the socio-economic losses (Lu et al., 2018; Doi et al., 2022). As for marine ecosystems, nIOD contributes to primary productivity in the Arabian Sea (Thushara and Vinayachandran, 2020) and has important implications for the habitat and distribution of tuna in the tropical western Indian Ocean (Wang et al., 2023). In addition, by affecting atmospheric circulation, nIOD contributes to the reduction of Antarctic sea ice (Wang et al., 2019).

The nIOD can also exert important influences on the climate in China. It decreases the rainfall in the central and southern parts of China (Yuan et al., 2008; Qiu et al., 2014; Zhang et al., 2022), whereas increases that in the Huanghe River (Yellow River) Basin and the southeastern part of China (Yuan et al., 2008). It also causes rainfall increase in fall in the Loess Plateau region of China (Xu et al., 2016). In addition, by affecting the atmospheric circulation in the Northwest Pacific Ocean, nIOD can cause significant increase in water temperature along the eastern coast of China, which in turn affects the ecological environment (Tan and Cai, 2018).

IOD is a phenomenon with significant seasonal phase lock-

Foundation item: The Basic Scientific Fund for National Public Research Institutes of China under contract No. 2022S02; the National Natural Science Foundation of China under contract No. 41976021.

*Corresponding author, E-mail: yfang@fio.org.cn

ing. A canonical IOD develops in summer, peaks in fall and decays in winter. However, recent studies reveal that a new type of IOD, early IOD, occurs more frequently under global warming (Du et al., 2013; Sun et al., 2015, 2022). It develops and decays one season earlier than canonical IOD. Early pIOD has been proved to be a major type of pIOD and have greater impact on summer rainfall than canonical pIOD (Weller et al., 2014). Although we have recognized the existence and importance of early pIOD, those of early nIOD and underlying mechanisms are not clear. Studying this issue will be helpful for improving the forecasting skill of IOD and better understanding its climate impacts. The rest of this paper is organized as follows. Section 2 introduces the datasets and methods. Section 3 describes the characteristics of early nIOD. Section 4 explores the triggering mechanism of early nIOD, and a summary is presented in Section 5.

2 Data and methods

The wind data used in this study were monthly data at 850 hPa from ERA5, the latest climate reanalysis produced by European Center for Medium-Range Weather Forecasts (ECMWF) (Hersbach et al., 2020). Wind anomalies were calculated with respect to the mean of 1959–2021. The 850 hPa wind was used because it was more suitable for studying the variations of the Indian summer monsoon and highly correlated with the surface wind, which could directly force the IOD (Sun et al., 2015). The UK Meteorological Office Hadley Center EN4.2.1 quality-controlled ocean temperature datasets (Good et al., 2013) were used to study subsurface temperature variations. Temperature anomalies were calculated with respect to the mean of 1959–2021.

Monthly SST from NOAA Extended Reconstructed Sea Surface Temperature Version 5 (ERSSTv5) and HadISST were also used (Huang et al., 2017; Rayner et al., 2003). SST anomalies were calculated with respect to the mean of 1959–2021, which were the same as that in subsurface temperature anomalies. Daily average, monthly mean, and long-term mean of outgoing longwave radiation (OLR) were calculated from the National Oceanic and Atmospheric Administration (NOAA) interpolated OLR product (Liebmann et al., 1996). The OLR anomaly is used as a proxy for large-scale convective activity over the Indian Ocean. The OLR anomalies were calculated with respect to the long-term mean of 1979–2021.

The Dipole Mode Index (DMI) is represented by the difference in SSTA between the tropical western Indian Ocean (10°S – 10°N , 50° – 70°E) and the tropical southeastern Indian

Ocean (10°S – 0° , 90° – 110°E) (Saji et al., 1999). The thermocline DMI is defined as the difference in thermocline depth (depth of the 20°C isotherm) anomalies in the same regions (Sun et al., 2022).

La Niña-related nIOD event is defined as occurrence when the averaged DMI during July–October and the averaged Niño-3.4 index during December–February both are below -0.5 standard deviations (s.d.). Early IOD event is distinguished with help of empirical orthogonal function (EOF) analysis, which identifies the dominant mode of equatorial zonal wind interannual variability. The EOF analysis follows the same method used in previous studies (Sun et al., 2015, 2022). The EOFs were calculated based on the time series of ERA5 equatorial zonal wind anomalies (averaged between 5°S and 5°N) yearly evolution from 1959 to 2021, thus the two-dimensional “spatial” part represents the seasonal evolution of zonal wind of individual years, and the “temporal” dimension shows the variation from 1959 to 2021. The linear trend was already removed before the calculation.

The first leading mode (EOF1) represents the equatorial easterly wind anomalies (EEWAs) evolution pattern during canonical pIODs, and peaks in fall. In the second leading mode (EOF2), the EEWAs set up in May and persist through boreal spring and summer, consistent with the EEWAs evolution associated with early pIOD shown in earlier studies (Sun et al., 2015, 2022). An early nIOD event is determined when the DMI and the second principal component (PC2) are both below -0.5 s.d. La Niña and delayed summer monsoon onset are independent of each other, but there is a possibility that they may appear in the same year. In this situation, La Niña and delayed summer monsoon onset both contribute to the development of nIOD. However, to make the results clear, only pure early nIOD and pure La Niña-related nIOD are discussed in this paper.

3 Characteristics of early nIOD

We examined the nIOD events over the period from 1959 to 2021, and totally 19 significant ones are identified (Fig. 1). Among them, seven are La Niña-related nIOD events, seven are early nIOD events, and another two nIOD events that occur with both types of nIOD events in the same year. Therefore, early nIOD and La Niña-related nIOD are the two dominant types of nIOD events, accounting for the vast majority (84.2%) of all the nIOD events.

The seasonal evolutions of early nIOD and La Niña-related nIOD are different from each other (Fig. 2). To clearly show the characteristics of the two types of nIOD, the events that occur

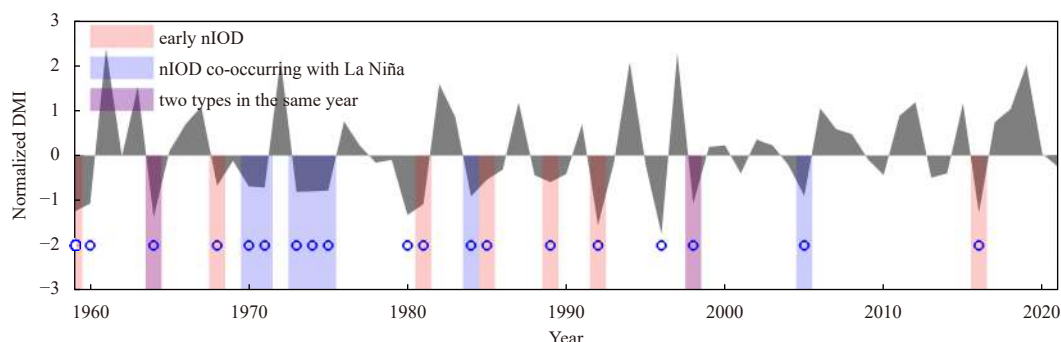


Fig. 1. The normalized time series of DMI (averaged during July–October, gray shading). The blue vertical bars indicate La Niña-related nIOD events. The pink bars indicate early nIOD events. The purple bars indicate both types of nIOD appear in the same year. All nIOD events are indicated by blue circles.

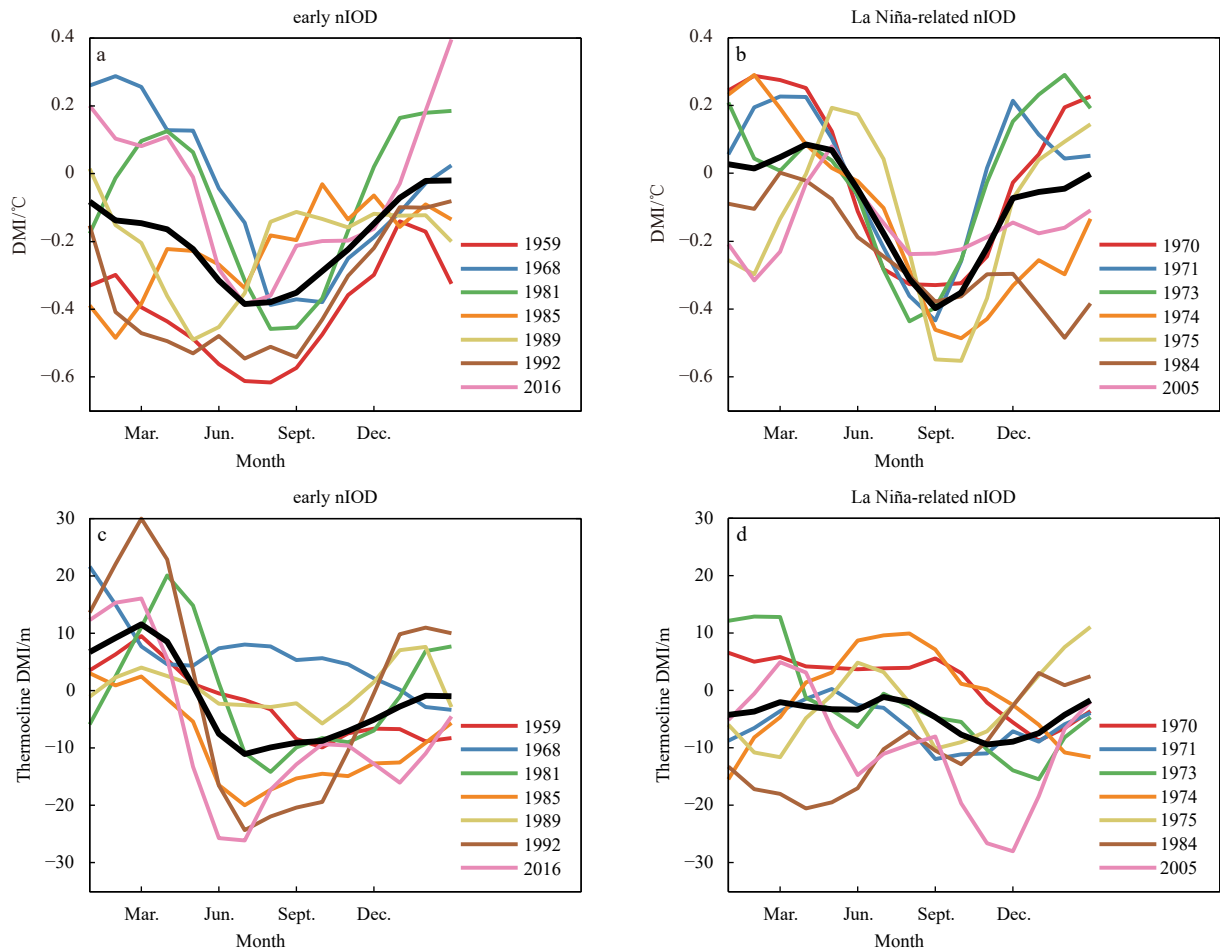


Fig. 2. Composite seasonal evolutions of DMI ($^{\circ}\text{C}$) during early nIOD (a) and La Niña-related nIOD (b), and composite seasonal evolutions of thermocline DMI (m) during early nIOD (c) and La Niña-related nIOD (d). The black curves are the mean values for the corresponding year.

with both types of nIOD in the same year are excluded in the composite analysis. The La Niña-related nIOD shows a typical seasonal cycle of IOD events, which develops in summer and peaks in fall. Whereas the temporal evolution of early nIOD is one season earlier than that of La Niña-related nIOD (Figs 2a and b). It develops in spring and peaks in summer. In fall, when La Niña-related nIOD peaks, early nIOD already decays. The intensity of early nIOD and La Niña-related nIOD are comparable to each other, both reaching about 0.4°C during their peaking phase. Such intensity is weaker than that of pIOD. Notably, El Niño-related pIOD is significantly stronger than La Niña-related nIOD, but the intensity difference between early pIOD and early nIOD is much smaller. This may relate to that the intensity of El Niño is markedly stronger than La Niña (Cai et al., 2021). During pIOD/nIOD events co-occurring with El Niño/La Niña, equatorial zonal wind anomalies in the Indian Ocean are remotely forced by the SST anomalies in the Pacific Ocean (Schott et al., 2009). Therefore, the IOD events triggered by El Niño and La Niña also show distinct intensity.

To analyze the subsurface variations, the thermocline DMI of early nIOD and La Niña-related nIOD are shown in Figs 2c and d. Early nIOD events are triggered by equatorial westerly wind anomalies which are associated with anomalous monsoon activity. This dynamical process is more clearly shown in the variations of thermocline DMI, which is influenced by dynamical processes

but not directly affected by surface heat flux. Therefore, the variations of thermocline DMI (Fig. 2c) are more consistent with the variations of DMI (Fig. 2a), and the develop and peak seasons are more clearly shown in Fig. 2c. The temporal evolution of thermocline DMI are generally consistent with the DMI during early nIOD. During La Niña-related nIOD, the subsurface anomalies evolve later than the surface anomalies. The DMI decays in November to December during La Niña-related nIOD, whereas the thermocline DMI peaks in these months and persists through winter. The phase difference between surface and subsurface variations also exists in ENSO-related pIOD. This feature is related to surface flux anomalies, which weakens the intensity of the IOD in fall (Sun et al., 2022). The magnitude of the thermocline DMI is similar for both types of nIOD events, which is about 10 m.

As shown in previous studies, all types of IOD events are tightly coupled to equatorial zonal wind anomalies. pIOD is accompanied by equatorial easterly wind anomalies, while nIOD is accompanied by EWWAs. Equatorial zonal wind anomalies can influence IOD through processes such as causing zonal temperature advection, inducing upwelling in the southeastern Indian Ocean, and triggering Kelvin and Rossby waves. To understand the role of EWWA in nIOD events, we composited the equatorial zonal wind during the two types of nIODs (Fig. 3). Significant EWWAs are found in both types of nIOD events, and they are

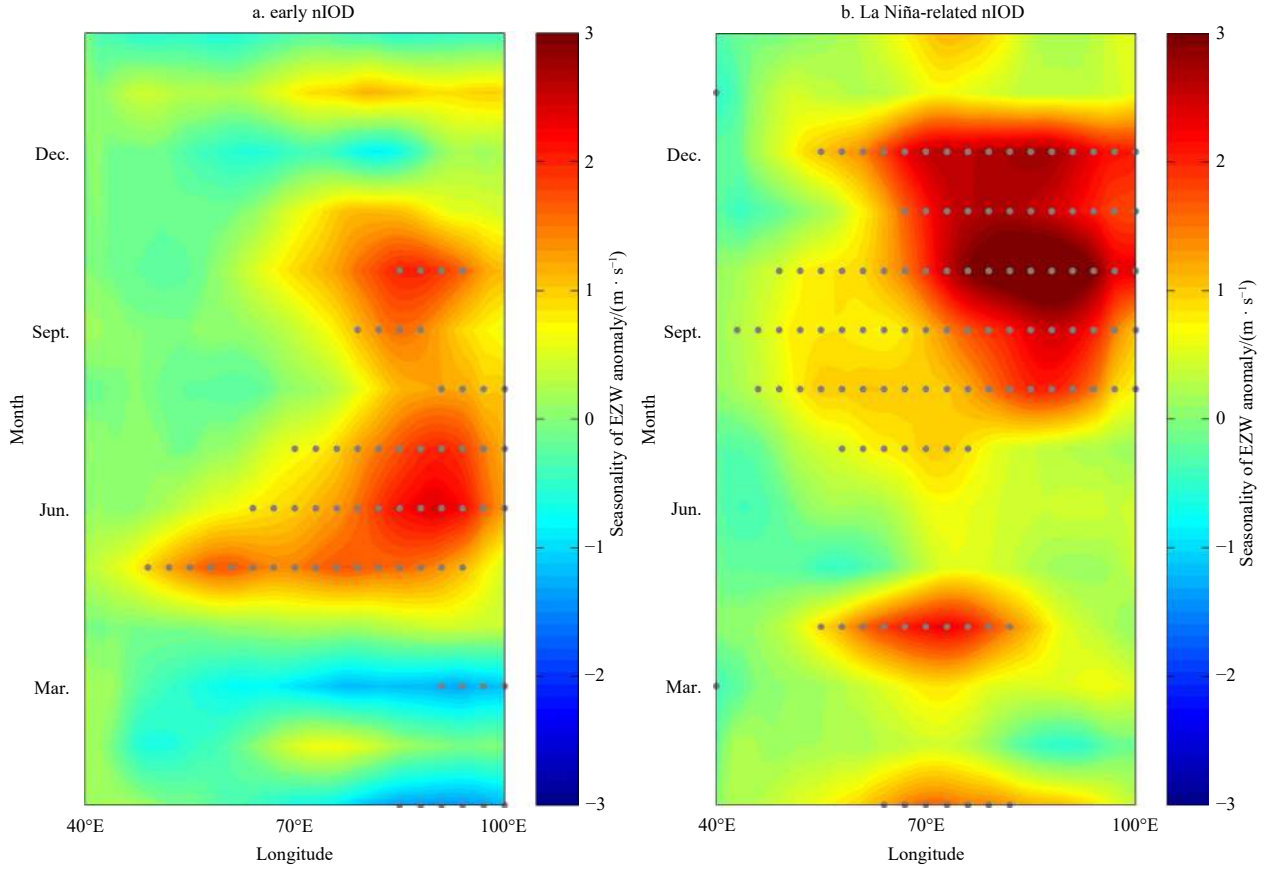


Fig. 3. Composite seasonal evolutions of equatorial zonal wind (EZW, averaged between 5°S and 5°N, m/s) anomalies during early nIOD (a) and La Niña-related nIOD (b). Values that exceed 90% confidence level are indicated by gray dots.

stronger in the eastern Indian Ocean than in the western Indian Ocean. During the early nIOD, the EWWA bursts out in May, and the intensity peaks within a month at around 2 m/s. The EWWA in the La Niña-related nIOD is stronger, reaching up to 3 m/s, but appears later—It starts to develop in summer and peaks in fall. The seasonal evolution of EWWA during the two types of nIOD events are consistent with the characteristics of the first and second EOF modes of the interannual zonal wind variation (Sun et al., 2015, 2022), implying that they are independent of each other, being the two dominant modes of interannual variability in the Indian Ocean.

4 Triggering mechanisms of early nIOD

According to previous studies, the outbreak of equatorial easterly wind anomaly in May, which is crucial for triggering early pIOD, is associated with the early onset of summer monsoon (Sun et al., 2015). In the years with early summer monsoon onset, the convection is anomalously enhanced in the Bay of Bengal (BoB) in late April to early May, causing early onset of summer monsoon in the BoB. Following this enhanced convection, suppressed convection appears in the southwestern Indian Ocean and gradually intensifies as its center propagates eastward, and arrives at the eastern equatorial Indian Ocean in mid-May. In response to the suppressed convection, easterly anomaly is established to the west of the suppressed convection center. That is why the EEWA always appears in May during early pIOD (Sun et al., 2015).

It is interesting to note that the spatial pattern of the wind an-

omaly during early nIOD in May (Fig. 4a) is generally opposite to that of the summer monsoon. This spatial pattern is also opposite to the one associated with early pIOD, implying that the early nIOD is very likely triggered by a process opposite to that of early pIOD, which is the delayed summer monsoon onset. During La Niña-related nIOD, the wind anomaly is not significant in this month. In order to verify this hypothesis, we analyzed the composite OLR (negative value represents enhanced convection) and wind anomalies during the summer monsoon onset period in early nIOD years.

Results show that the convection is anomalously weakened in the BoB in late April and early May (Figs 5a–c)—The period when summer monsoon usually onsets in the region. Since the monsoon onset is always accompanied by significant local convection enhancement, weak convection in this season implies that the convection necessary for monsoon onset develops later than normal. Figure 5 shows that the suppressed convection lasts from late April to early May causes a delay in monsoon onset. As a result, the westerly monsoon winds that should have appeared in this season are absent, resulting in anomalous easterly in the Arabian Sea and the BoB and anomalous westerly in the southern Indian Ocean (Figs 5e–g). Following the suppressed convection, an enhanced phase of convection develops in the southwestern Indian Ocean and propagates eastward (Fig. 5d). In response to this convection center, westerly anomalies are generated in the equatorial Indian Ocean (Fig. 5h). The westerly anomaly can further induce downwelling in eastern Indian Ocean and upwelling in western Indian Ocean, thus causing warm temper-

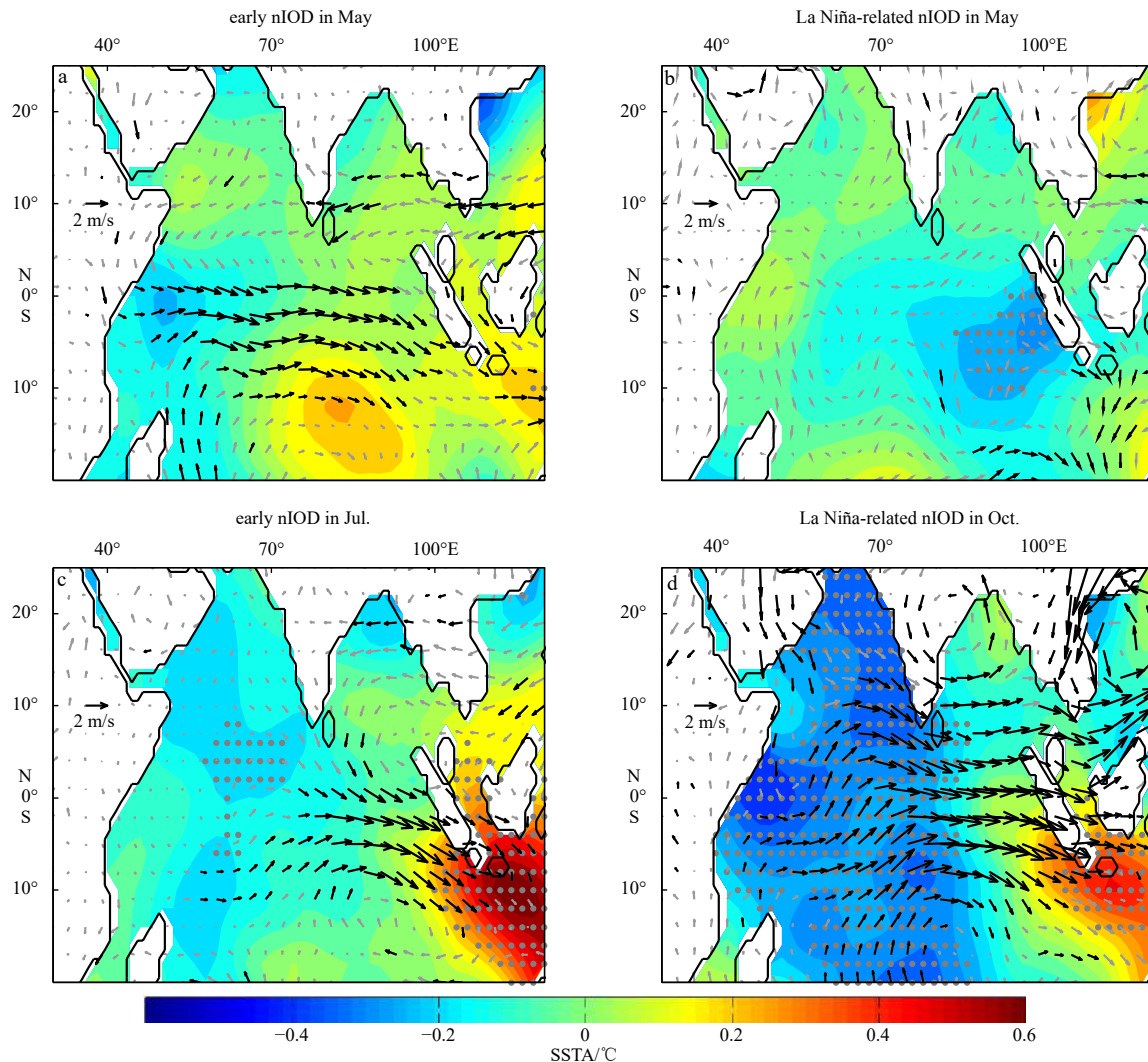


Fig. 4. Composites of SSTA ($^{\circ}\text{C}$, color shading) and 850 hPa wind anomalies (m/s, vectors) in May of early nIOD (a) and La Niña-related nIOD (b), in the peak month (July) of early nIOD (c) and in the peak month (October) of La Niña-related nIOD (d). Wind vectors and SSTA values that exceed the 90% confidence level are shown in black arrows and gray dots, respectively.

ature advection to the east, triggering the early nIOD.

After early nIOD is triggered, the anomalous east-west SST gradient develops under Bjerknes feedback, and peaks in summer. In the absence of persistent external forcing, early nIOD decays in fall. It is worth to note that the wind anomaly associated with the early nIOD is similar to the winter monsoon pattern (Figs 4a and c), but significantly different from the wind anomaly associated with the La Niña-related nIOD, which is symmetric about the equator with two cyclones in the northern and southern Indian Ocean (Fig. 4d). In La Niña-related nIOD, the westerly anomalies cover the entire equatorial Indian Ocean, causing significant SST anomalies in both pole of nIOD. Whereas during early nIOD, the westerly anomalies are confined to the central and eastern equatorial Indian Ocean. As for the spatial pattern of SSTA, the intensities of east pole and west pole are not symmetric in early nIOD—The eastern warming is much stronger than the western cooling. While in La Niña-related nIOD, the magnitude of SSTA in the two poles are basically the same. Owing to the different triggering mechanisms, the characteristics of the two types of nIOD are fundamentally different from each other in their spatial pattern and temporal evolution.

5 Summary

The characteristics and triggering mechanisms of early nIOD were investigated in this study. Results show that the early nIOD and the La Niña-related nIOD are two major types of nIOD. The magnitude of early nIOD is basically same as that of La Niña-related nIOD, but the seasonal cycle and spatial pattern of early nIOD are fundamentally different from those of La Niña-related nIOD. The early nIOD starts to develop in May, peaks in summer, and decays in fall, the entire life cycle is about one season earlier than that of the La Niña-related nIOD. Spatial pattern of the wind anomaly associated with early nIOD exhibits a winter monsoon-like pattern, fundamentally different from the one associated with La Niña-related nIOD, which is symmetric about the equator. SST response in the east pole during the peak of early nIOD is much stronger than that in the west pole, while in La Niña-related nIOD, the magnitude of the SSTA in the two poles are basically the same.

The triggering mechanism of early nIOD is similar to that of early pIOD (both are induced by the variation of summer monsoon onset), but the atmospheric and oceanic processes involved in the two mechanisms are opposite. Delay in summer monsoon onset causes a winter monsoon-like pattern in the

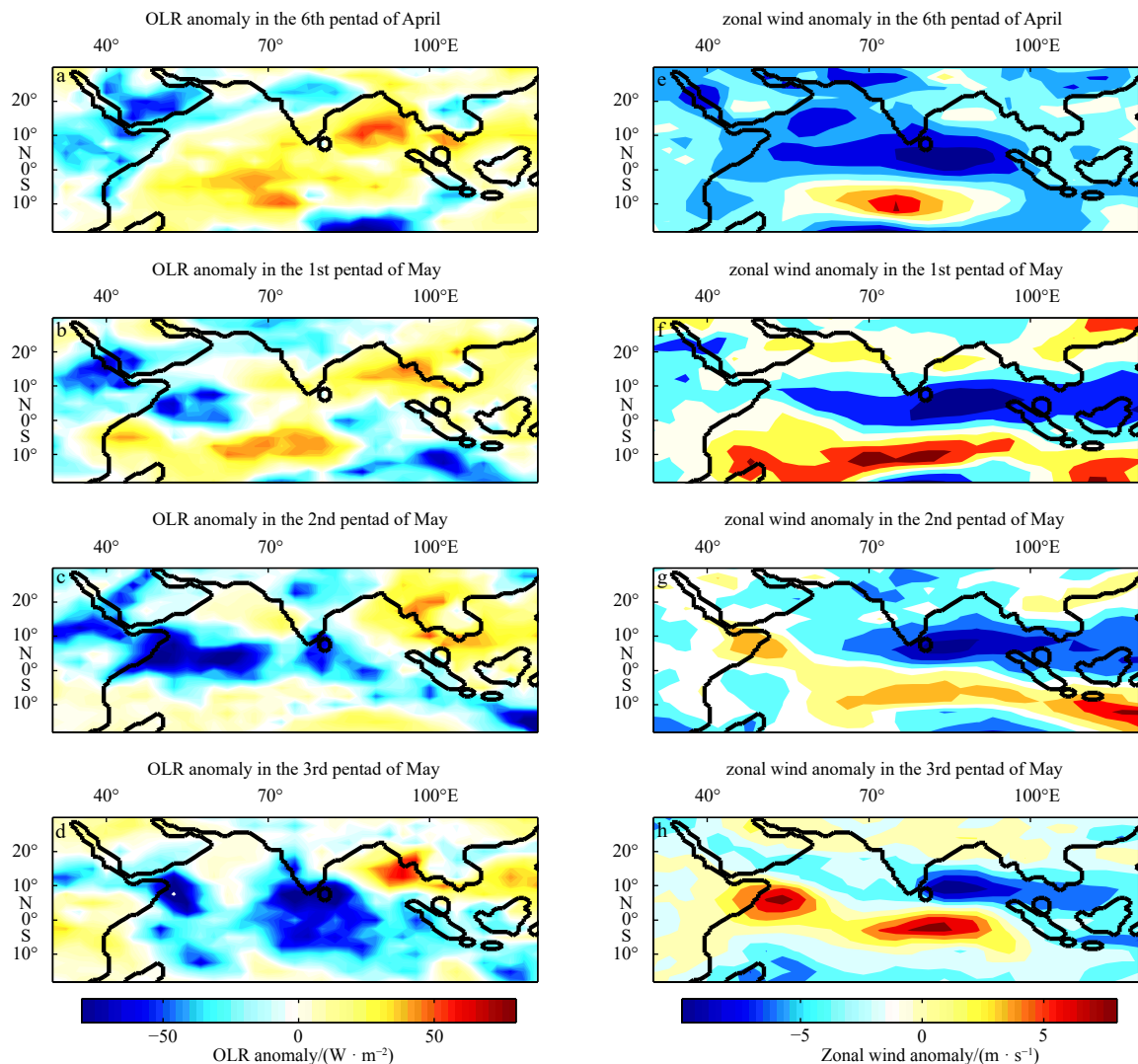


Fig. 5. Composite outgoing longwave radiation (OLR) anomaly in spring (from the 6th pentad of April to the 3rd pentad of May) during early nIOD (a-d), and composite zonal wind anomalies at 850 hPa in spring (from the 6th pentad of April to the 3rd pentad of May) during early nIOD (e-h).

wind anomaly in the tropical Indian Ocean in spring. The westerly wind anomalies push the water in west equatorial region to the east, and deepen the thermocline in southeastern equatorial Indian Ocean, causing anomalous warming in SST in the region. The east-west SST gradient may further enhance the westerly wind anomaly. The delay in summer monsoon onset and associated Bjerknes feedbacks are responsible for occurrence of the early nIOD events. Understanding the characteristics and mechanism of the early nIOD is important for understanding the climate variability and its impacts in tropical Indian ocean, and also helpful for improving the skill of climate prediction in the region.

References

- Cai Wenju, Santoso A, Collins M, et al. 2021. Changing El Niño–Southern Oscillation in a warming climate. *Nature Reviews Earth & Environment*, 2: 628–644., doi: [10.1038/s43017-021-00199-z](https://doi.org/10.1038/s43017-021-00199-z)
- Doi T, Behera S K, Yamagata T. 2022. On the predictability of the extreme drought in east Africa during the short rains season. *Geophysical Research Letters*, 49(22): e2022GL100905, doi: [10.1029/2022GL100905](https://doi.org/10.1029/2022GL100905)
- Du Yan, Cai Wenju, Wu Yanling. 2013. A new type of the Indian Ocean Dipole since the mid-1970s. *Journal of Climate*, 26(3): 959–972, doi: [10.1175/JCLI-D-12-00047.1](https://doi.org/10.1175/JCLI-D-12-00047.1)
- Good S A, Martin M J, Rayner N A. 2013. EN4: quality controlled ocean temperature and salinity profiles and monthly objective analyses with uncertainty estimates. *Journal of Geophysical Research: Oceans*, 118(12): 6704–6716, doi: [10.1002/2013JC009067](https://doi.org/10.1002/2013JC009067)
- Hatmaja R B, Rusmanansari A H, Radjawane I M. 2019. The dynamics of negative Indian Ocean Dipole (nIOD) and its relation to the anomalous high rainfall in West Java Province, Indonesia. *IOP Conference Series: Earth and Environmental Science*, 303(1): 012004, doi: [10.1088/1755-1315/303/1/012004](https://doi.org/10.1088/1755-1315/303/1/012004)
- Hersbach H, Bell B, Berrisford P, et al. 2020. The ERA5 global reanalysis. *Quarterly Journal of the Royal Meteorological Society*, 146(700): 1999–2049, doi: [10.1002/qj.3803](https://doi.org/10.1002/qj.3803)
- Huang Boyin, Thorne P W, Banzon V F, et al. 2017. Extended reconstructed sea surface temperature, version 5 (ERSSTv5): upgrades, validations, and intercomparisons. *Journal of Climate*, 30(20): 8179–8205, doi: [10.1175/JCLI-D-16-0836.1](https://doi.org/10.1175/JCLI-D-16-0836.1)
- Liebmann B, Smith C A. 1996. Description of a complete (interpolated) outgoing longwave radiation dataset. *Bulletin of the American Meteorological Society*, 77(6): 1275–1277
- Lim E P, Hendon H H. 2017. Causes and predictability of the negative Indian Ocean dipole and its impact on La Niña during 2016. *Scientific Reports*, 7(1): 12619, doi: [10.1038/s41598-017-12674-z](https://doi.org/10.1038/s41598-017-12674-z)

- Lu Bo, Ren Hongli, Scaife A A, et al. 2018. An extreme negative Indian Ocean dipole event in 2016: dynamics and predictability. *Climate Dynamics*, 51(1/2): 89–100, doi: [10.1007/s00382-017-3908-2](https://doi.org/10.1007/s00382-017-3908-2)
- Qiu Yun, Cai Wenju, Guo Xiaogang, et al. 2014. The asymmetric influence of the positive and negative IOD events on China's rainfall. *Scientific Reports*, 4: 4943, doi: [10.1038/srep04943](https://doi.org/10.1038/srep04943)
- Rayner N A, Parker D E, Horton E B, et al. 2003. Global analyses of sea surface temperature, sea ice, and night marine air temperature since the late nineteenth century. *Journal of Geophysical Research: Atmospheres*, 108(D14): 4407, doi: [10.1029/2002JD002670](https://doi.org/10.1029/2002JD002670)
- Risbey J S, Pook M J, McIntosh P C, et al. 2009. On the remote drivers of rainfall variability in Australia. *Monthly Weather Review*, 137(10): 3233–3253, doi: [10.1175/2009MWR2861.1](https://doi.org/10.1175/2009MWR2861.1)
- Saji N H, Goswami B N, Vinayachandran P N, et al. 1999. A dipole mode in the tropical Indian Ocean. *Nature*, 401(6751): 360–363, doi: [10.1038/43854](https://doi.org/10.1038/43854)
- Saji N H, Yamagata T. 2003. Possible impacts of Indian Ocean Dipole mode events on global climate. *Climate Research*, 25(2): 151–169, doi: [10.3354/cr025151](https://doi.org/10.3354/cr025151)
- Schott F A, Xie S P, McCreary J P. 2009. Indian Ocean circulation and climate variability. *Reviews of Geophysics*, 47(1): RG1002., doi: [10.1029/2007RG000245](https://doi.org/10.1029/2007RG000245)
- Sun Shuangwen, Fang Yue, Zu Yongcan, et al. 2022. Increased occurrences of early Indian Ocean Dipole under global warming. *Science Advances*, 8(47): eadd6025, doi: [10.1126/sciadv.add6025](https://doi.org/10.1126/sciadv.add6025)
- Sun Shuangwen, Lan Jian, Fang Yue, et al. 2015. A triggering mechanism for the Indian Ocean Dipoles independent of ENSO. *Journal of Climate*, 28(13): 5063–5076, doi: [10.1175/JCLI-D-14-00580.1](https://doi.org/10.1175/JCLI-D-14-00580.1)
- Tan Hongjian, Cai Rongshuo. 2018. What caused the record-breaking warming in East China Seas during August 2016?. *Atmospheric Science Letters*, 19(10): e853, doi: [10.1002/asl.853](https://doi.org/10.1002/asl.853)
- Thushara V, Vinayachandran P N. 2020. Unprecedented surface chlorophyll blooms in the southeastern Arabian Sea during an extreme negative Indian Ocean Dipole. *Geophysical Research Letters*, 47(13): e2019GL085026, doi: [10.1029/2019GL085026](https://doi.org/10.1029/2019GL085026)
- Wang Guomin, Hendon H H, Arblaster J M, et al. 2019. Compounding tropical and stratospheric forcing of the record low Antarctic sea-ice in 2016. *Nature Communications*, 10(1): 13, doi: [10.1038/s41467-018-07689-7](https://doi.org/10.1038/s41467-018-07689-7)
- Wang Yang, Zhang Fang, Geng Zhe, et al. 2023. Effects of climate variability on two commercial tuna species abundance in the Indian Ocean. *Fishes*, 8(2): 99, doi: [10.3390/fishes8020099](https://doi.org/10.3390/fishes8020099)
- Webster P J, Moore A M, Loschnigg J P, et al. 1999. Coupled ocean-atmosphere dynamics in the Indian Ocean during 1997–98. *Nature*, 401(6751): 356–360, doi: [10.1038/43848](https://doi.org/10.1038/43848)
- Weller E, Cai Wenju, Du Yan, et al. 2014. Differentiating flavors of the Indian Ocean Dipole using dominant modes in tropical Indian Ocean rainfall. *Geophysical Research Letters*, 41(24): 8978–8986, doi: [10.1002/2014GL062459](https://doi.org/10.1002/2014GL062459)
- WMO. 2017. WMO Statement on the State of the Global Climate in 2016. Geneva: World Meteorological Organization
- Xu Kang, Zhu Congwen, Wang Weiqiang. 2016. The cooperative impacts of the El Niño-southern oscillation and the Indian Ocean dipole on the interannual variability of autumn rainfall in China. *International Journal of Climatology*, 36(4): 1987–1999, doi: [10.1002/joc.4475](https://doi.org/10.1002/joc.4475)
- Yuan Yuan, Yang Hui, Zhou Wen, et al. 2008. Influences of the Indian Ocean Dipole on the Asian summer monsoon in the following year. *International Journal of Climatology*, 28(14): 1849–1859, doi: [10.1002/joc.1678](https://doi.org/10.1002/joc.1678)
- Zhang Ling, Shi Ruizhi, Fraedrich K, et al. 2022. Enhanced joint effects of ENSO and IOD on Southeast China winter precipitation after 1980s. *Climate Dynamics*, 58(1/2): 277–292, doi: [10.1007/s00382-021-05907-5](https://doi.org/10.1007/s00382-021-05907-5)